


Please cite the Published Version

Saied, Osama, Li, Xingwang and Rabie, Khaled M  (2022) DFT spread-optical pulse amplitude modulation for visible light communication systems. IEEE Access, 10. pp. 15956-15967. ISSN 2169-3536

DOI: <https://doi.org/10.1109/ACCESS.2022.3147209>

Publisher: IEEE

Version: Published Version

Downloaded from: <https://e-space.mmu.ac.uk/632930/>

Usage rights:  [Creative Commons: Attribution 4.0](https://creativecommons.org/licenses/by/4.0/)

Additional Information: This is an open access article which originally appeared in IEEE Access

Enquiries:

If you have questions about this document, contact openresearch@mmu.ac.uk. Please include the URL of the record in e-space. If you believe that your, or a third party's rights have been compromised through this document please see our Take Down policy (available from <https://www.mmu.ac.uk/library/using-the-library/policies-and-guidelines>)

DFT Spread-Optical Pulse Amplitude Modulation for Visible Light Communication Systems

OSAMA SAIED¹, XINGWANG LI², (Senior Member, IEEE),
AND KHALED M. RABIE³, (Senior Member, IEEE)

¹Computer Engineering Department, Biruni Remote Sensing Center (BRSC), Tripoli, Libya

²School of Physics and Electronic Information Engineering, Henan Polytechnic University, Jiaozuo 454000, China

³Faculty of Science and Engineering, Manchester Metropolitan University, Manchester M15 5GD, U.K.

Corresponding author: Osama Saied (osama.dhawi.saied@hotmail.com)

ABSTRACT DC-biased optical orthogonal frequency division multiplexing (DCO-OFDM) has been proposed in visible light communication (VLC) to overcome the limited modulation bandwidth of light emitting diode (LED). Due to the implementation of the inverse fast Fourier transform at the DCO-OFDM transmitter, DCO-OFDM suffers from its high peak-to-average power ratio (PAPR), which restricts its use in some VLC applications, especially where the optical power efficiency is a crucial requirement. That is because the LEDs used in VLC systems have a limited optical power-current linear range. To this end, a novel discrete Fourier transform spread-optical pulse amplitude modulation (DFTS-OPAM) signal scheme based on the single carrier-interleaved frequency division multiple access (SC-IFDMA) signal is introduced in this paper to address the high PAPR issue of OFDM. DFTS-OPAM is achieved by considering a PAM as an SC-IFDMA data symbol and duplicate the output vector of the fast Fourier transform at the SC-IFDMA transmitter side. Simulation results show that the PAPR of the proposed scheme is 7 dB lower than that of DCO-OFDM. Furthermore, this significant PAPR improvement is experimentally investigated where the practical results show that the proposed scheme can provide more 2.5 dB reduction in the average transmitted power requirement compared to DCO-OFDM and can subsequently increase the maximum achieved distance between the transmitter and the receiver up to 44%.

INDEX TERMS Single carrier frequency division multiple access, DC-biased optical orthogonal frequency division multiplexing, visible light communication, peak-to-average power ratio, light-emitting diode, dynamic range.

I. INTRODUCTION

Visible light communications (VLCs) have received a great deal of research attention as a promising candidate for future broadband networks by utilizing white light emitting diodes (LEDs) in the existing solid-state lighting (SSL) infrastructure. LEDs offer multiple usages such as illumination, high-speed data transmission and localization in various applications [1]–[3]. Compared to the wireless radio frequency (RF) technologies, VLC systems are energy-efficient, cost-effective, and ideal for use in hospitals, aircraft cabins or in petrochemical industries since it does not interfere with other radio frequency (RF) systems nor induces any health issues. Furthermore, VLCs occupy an unregulated portion of the electromagnetic spectrum and offer a large transmission bandwidth [1]–[4]. Although the wavelength of the visible

light ranges from 380 to 780 nm (i.e., offers a bandwidth of up to 300 THz), the 3 dB modulation bandwidth ($3 dB_{BW}$) of the standard high-power white phosphor LED (PWLED) that is used for illumination is only a few MHz, which limits the maximum achievable VLC data rate [1], [2]. To expand the $3 dB_{BW}$ of the LED, optical blue filtering was employed at the receiver (Rx) side to filter out the slow yellowish component of the LEDs [5]. In addition to the optical blue filtering, pre-and post-equalization methods were also proposed to extend the $3 dB_{BW}$ of the LEDs [6]–[8]. For example, using pre-and post-equalizations with the emitter degenerated LED driver increase the $3 dB_{BW}$ of the blue, red, and green LEDs by 174, 180, and 145 MHz, respectively [6]. However, these methods cause a significant reduction in the received signal-to-noise ratio (SNR) [9], [10].

Alternatively, a few diversity and complex techniques have been proposed to compensate the LED modulation bandwidth limitation and consequently improve the VLC data rate.

The associate editor coordinating the review of this manuscript and approving it for publication was Jiajie Fan¹.

Multiple input multiple output (MIMO) techniques have been studied to increase the VLC data rate. For example, higher achievable capacity results with spatial multiplexing MIMO method and higher diversity gains with repetition coding MIMO as compared to single input single output (SISO) systems are reported in [11]. The MIMO techniques have also been considered in conjunction with multi-carrier transmission in [12], [13] and the link capacity has been improved with adaptive transmission in frequency selective VLC channels. In addition to MIMO techniques, multi-level modulation schemes including M-ary pulse amplitude modulation scheme has also employed in VLC to enhance its data rate as shown in [14]. PAM-single-carrier with frequency-domain equalization (PAM-SCFDE) has also been introduced in VLC systems to overcome the multipath issue and consequently increase the VLC data rates [15]. Investigating the bit and power loading features of multi carrier modulation (MCM) signals such as orthogonal frequency division multiplexing (OFDM) in VLC systems has demonstrated a significant data rate improvement. For instance, more than 15 Gbps data rates has been recently reported in [16] when the OFDM based on wavelength division multiplexing of four LEDs (i.e., RGBY) is employed.

The VLC systems uses intensity modulation and direct detection (IM/DD) where the signals are modulated to the light intensity. As a result, a bipolar and complex signal such as the traditional OFDM signal must be first converted into real and unipolar signal before modulating an LED. To make signal real and unipolar in DC-biased optical OFDM (DCO-OFDM), Hermitian Symmetry (HS) is imposed before inverse fast Fourier transform (IFFT) at a cost of halving the available electrical bandwidth [17] followed by addition of a DC-bias [18]. However, adding a DC-bias to a large peak to average power ratio (PAPR) signal, and passing it through the limited LED linear dynamic range makes this scheme unsuitable in some VLC applications where the power efficiency is a crucial requirement such as in dimming control [19]. Alternatively, the IFFT properties have been again exploited to make the OFDM signal unipolar without any DC-bias requirements [20], [21]. This comes at the cost of halving the spectral efficiency in comparison to the DCO-OFDM scheme which is achieved by keeping the real part of the data symbols to be blank in the pulse amplitude modulated discrete multitone (PAM-DMT) or by modulating only the odd subcarriers in asymmetrically clipped optical OFDM (ACO-OFDM). Despite their lower spectral efficiency compared to DCO-OFDM, ACO-OFDM and PAM-DMT still possess a high PAPR compared to single carrier modulation (SCM) [18]. Furthermore, the DC-bias may be needed in VLC systems to provide an illumination service and to remove the effect of the pulse shaping filter, which can convert unipolar signals to bipolar ones [18], [22].

Implementing FFT and interleaving mapping before the implementation of the IFFT at the OFDM transmitter (Tx) results in a special single carrier modulation scheme known as single carrier-interleaved frequency division multiple access

(SC-IFDMA) [23], [24]. Such signal has almost the same features as OFDM (i.e., bit and power loading and reduce inter-symbol interference) but a low PAPR signal such as an SCM signal [25]–[28]. However, the SC-IFDMA is mainly proposed as a means to improve the OFDM PAPR signal in the RF domain and has recently been modified to make it suitable for IM/DD based VLC systems [29]–[35].

The ACO-single carrier frequency-domain equalization (ACO-SCFDE) and the unipolar pulse amplitude modulation frequency division multiplexing (UPAM-FDM) are the two SC-IFDMA modified schemes that have recently been proposed to make the SC-IFDMA suitable for VLC systems [29]–[31]. To make the SC-IFDMA signal a real signal, its FFT output subcarriers at its Tx should be symmetrically conjugated. This was achieved in the U-PAM-FDM by considering a PAM as an SC-IFDMA data symbol which results in a symmetrically output FFT conjugated subcarriers excluding the first and the middle ones. To make all the U-PAM-FDM output FFT subcarriers are symmetrically conjugated, a subcarrier conjugate (SCG) block is added after the FFT implementation at the U-PAM-FDM Tx where a copy of the first and the middle subcarriers are respectively inserted after the middle and the last ones [31]. On the other hand, the output FFT subcarriers of the ACO-SCFDE are imposed to HS at the Tx to satisfy the condition for the values to be real [29], [30]. However, the implementation of the HS and the SCG at the Tx of the ACO-SCFDE and the U-PAM-FDM leads to the increase in their PAPR values in comparison to the traditional SC-IFDMA [31], [32].

Optical single carrier-interleaved FDM (OSC-IFDM) scheme was introduced in [33]–[35] to make the PAPR value of the optical SC-IFDMA as low as the PAPR value of the traditional (RF) SC-IFDMA by adopting the SC-IFDMA for VLC systems without any HS or SCG requirements. This is achieved by the time domain SC-IFDMA symbol to be repeated twice (i.e., setting the interleaving mapping factor in the frequency domain to be 2) [35]. For this, the first half of this symbol is used to transmit the real-time domain samples while the second half is used for the imaginary part. However, unlike all other modified SC-IFDMA schemes, the 1st OSC-IFDM subcarrier (DC term) had to be a modulated which is affected by the DC-bias and consequently affect all the samples in the time domain. This makes SC-IFDMA scheme difficult to implement in a real time [35]. Note that in VLC systems, the DC level is unmodulated as it uses for turning on the LEDs, dimming or shifting the bias levels [1], [2], [19].

In this study, we propose a new discrete Fourier transform spread-optical pulse amplitude modulation (DFTS-OPAM) signaling scheme. Unlike other optical SC-IFDMA schemes, DFTS-OPAM achieves a low PAPR comparable to PAPR of the RF SC-IFDMA without compromising the system performance. In DFTS-OPAM, interleaving mapping block of the SC-IFDMA at the Tx is replaced by the repeating mapping (RM). In the RM block, the output FFT vector is repeated before the IFFT block, which makes the even

IFFT output samples similar to the input data symbols, and the odd output samples zeros. Therefore, making the data symbols real (i.e., PAM symbols) results in real IFFT output samples suitable for IM/DD, at the cost of halving the spectral efficiency. Since the odd samples do not carry any data in DFTS-OPAM, another DFTS-OPAM signal can be transmitted in these odd samples using the time division multiple access (TDMA) technique (i.e., providing a high data rate for multiple access services). In addition, these unused DFTS-OPAM samples can be utilized for illumination, time-domain equalization, positioning and localization. Furthermore, due to the presence of the RM block, any affected subcarrier in DFTS-OPAM can be easily compensated.

The simulation results shows that the PAPR value of the DFTS-OPAM scheme is ~ 7 dB lower than the DCO-OFDM scheme. Furthermore, the effect of PAPR reduction is practically investigated, with the results showing the possible increase in the maximum achieved distance between the Tx and the Rx by up to 44% for the proposed scheme in comparison to the DCO-OFDM scheme.

The remainder of this paper is structured as follows. Section II presents the proposed DFTS-OPAM scheme. The simulation and the experimental results obtained for the proposed scheme are analyzed and discussed in Section III and Section IV, respectively. Finally, conclusions are drawn in Section V.

II. DISCRETE FOURIER TRANSFORM SPREAD OPTICAL PULSE AMPLITUDE MODULATION

In this section, the signal processing of the DFTS-OPAM scheme is illustrated and explained in detail where the reduction in the PAPR of this scheme is mathematically established and analyzed.

A. DFTS-OPAM TX

Fig. 1 shows an example of the DFTS-OPAM Tx signal processing procedure. First, random serial binary input bits $b_i(t)$ are converted to parallel and mapped to real PAM signal i.e., $\mathbf{p} = \{p_0, p_1, p_2, \dots, p_{M-1}\}$, and M is the number of transmitted data symbols. The real vector \mathbf{p} is then converted to a frequency domain by implementing the FFT operation, where the resulting FFT output sub-carriers (P) are conjugated symbols as shown in Fig. 1 and established below:

$$P_k = \sum_{m=0}^{M-1} p_m e^{-\frac{j2\pi mk}{M}} \quad (1)$$

$$\begin{aligned} P_{M-k} &= \sum_{m=0}^{M-1} p_m e^{-j(\frac{2\pi m}{M})(M-k)} \\ &= \sum_{m=0}^{M-1} p_m e^{-j(2\pi m - \frac{2\pi mk}{M})} \\ &= \sum_{m=0}^{M-1} p_m e^{\frac{j2\pi mk}{M}} \end{aligned} \quad (2)$$

From (1) and (2), it can be seen that each k^{th} subcarrier is conjugate of the $M - k^{th}$ subcarrier (i.e., $P_k = P_{M-k}^*$), for \mathbf{p} is a real vector. Subsequently, \mathbf{P} is repeated twice by passed through the RM process, where the new frequency domain output symbol vector (\mathbf{X}) has a length of $N = 2M$, which is defined as:

$$\begin{aligned} \mathbf{X} &= \{p_0, p_1, p_2, \dots, p_{M-1}, p_0, p_1, p_2, \dots, p_{M-1}\} \\ \mathbf{X} &= \{X_0, X_1, X_2, X_3, X_4, \dots, X_{N-1}\} \end{aligned} \quad (3)$$

\mathbf{X} is then converted back to the time domain samples vector (\mathbf{x}) using IFFT. However, because the IFFT operation is implemented before the RM and FFT blocks, \mathbf{x} has as low a PAPR value as that of a SCM scheme, as shown below:

$$\begin{aligned} x_n &= \frac{1}{N} \sum_{l=0}^{N-1} X_l e^{\frac{j2\pi ln}{N}} \\ x_n &= \frac{1}{N} \left[\sum_{l=0}^{\frac{N}{2}-1} X_l e^{\frac{j2\pi ln}{N}} + \sum_{l=\frac{N}{2}}^{N-1} X_l e^{\frac{j2\pi ln}{N}} \right] \end{aligned} \quad (4)$$

From (4), the following equation can be deduced:

$$\begin{aligned} x_n &= \frac{1}{N} \left[\sum_{k=0}^{M-1} P_l e^{\frac{j2\pi nk}{N}} + \sum_{k=0}^{M-1} P_k e^{\frac{j2\pi n(M+k)}{N}} \right] \\ x_n &= \frac{1}{N} \left[\sum_{k=0}^{M-1} P_l e^{\frac{j2\pi nk}{N}} + \sum_{k=0}^{M-1} P_k e^{j(\pi n + \frac{2\pi nk}{N})} \right] \end{aligned} \quad (5)$$

Thus, the odd and even samples of \mathbf{x} respectively defined as:

$$\begin{aligned} x_{n_Odd} &= \frac{1}{N} \left[\sum_{k=0}^{M-1} P_l e^{\frac{j2\pi nk}{N}} - \sum_{k=0}^{M-1} P_l e^{\frac{j2\pi nk}{N}} \right] = 0 \quad (6) \\ x_{n_Even} &= \frac{1}{2M} \left[\sum_{k=0}^{M-1} P_l e^{\frac{j2\pi nk}{M}} + \sum_{k=0}^{M-1} P_l e^{\frac{j2\pi nk}{M}} \right] \\ x_{n_Even} &= \frac{1}{M} \sum_{k=0}^{M-1} P_l e^{\frac{j2\pi nk}{M}} \end{aligned} \quad (7)$$

From (6) and (7), one can see that x_{n_Even} is a repeated signal of p_m , while no samples are carried on x_{n_Odd} (i.e., $x_{n_Odd} = 0$ (see Fig. 1)). Note that, as DFTS-OPAM uses PAM as a modulation technique, its spectral efficiency is a half of that of the DCO-OFDM scheme (i.e., has the same spectral efficiency as ACO-OFDM). Furthermore, because of the RM process, any distorted subcarrier in this scheme can be easily recovered. Finally, \mathbf{x} is passed through the parallel to serial (P/S) converter, cyclic prefix (CP) insertion, digital analogue converter (DAC), low pass filter (LPF), DC-bias, clipping, and electrical to optical converter (EOC) blocks.

B. DFTS-OPAM RX

Fig. 2 depicts the block diagram of the DFTS-OPAM Rx. Firstly, the transmitted optical signal is converted to an electrical signal by the photodetector (PD). Furthermore, to account for shot noise due to the photocurrent fluctuations

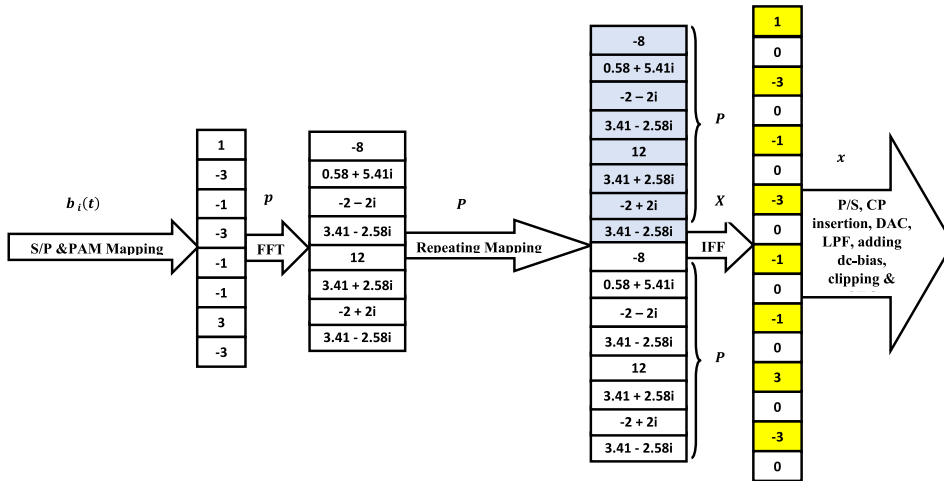


FIGURE 1. An example of the DFTS-OPAM Tx signal processing procedure.

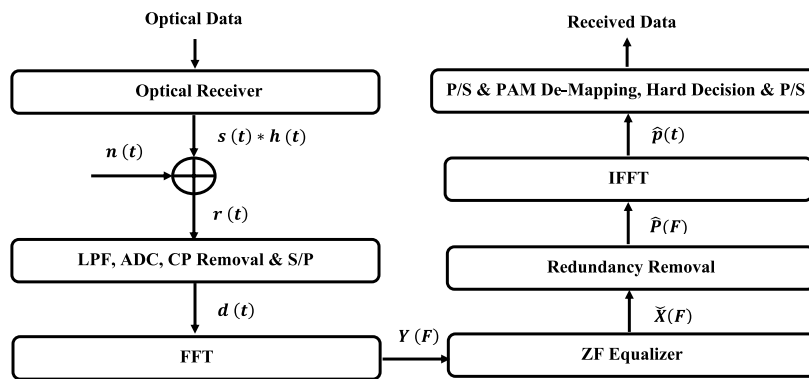


FIGURE 2. Block diagram of the DFTS-OPAM Rx.

and thermal noise due to the receiver electronics, additive white Gaussian noise (AWGN) is added to the electrical signal. Hence, the resulting analogue electrical signal $r(t)$ is given by $r(t) = s(t) * h(t) + n(t)$, where $s(t)$ is the transmitted electrical signal, $h(t)$ is the time domain system impulse response, $n(t)$ is the AWGN, and the symbol $*$ denotes the linear convolution operation (note that the PD is considered to be ideal (i.e., PD responsivity = 1)). $r(t)$ is then passed through the LPF, analogue digital converter (ADC), CP removal, and serial to parallel (S/P) blocks, where the resulting digital signal $d(t)$ of the aforementioned processes is converted to the frequency domain $Y(F)$ by FFT operation. Note that, since CP converts the linear convolution induced by the system to circular convolution (i.e., multiplication in the frequency domain), $Y(F)$ is given by:

$$Y(F) = X(F)H(F) + N(F) \quad (8)$$

where, $H(F)$ is the transfer function of the system. The transmitted signals are subsequently estimated by implementing the zero-forcing (ZF) equalizer, i.e.

$$\check{X}(F) = \frac{Y(F)}{\hat{H}(F)} \quad (9)$$

where, $\hat{H}(F)$ is the estimated transfer function of the system. If the full knowledge of the channel state is known (i.e., $\hat{H}(F) \approx H(F)$), then

$$\check{X}(F) = X(F) \quad (10)$$

After that, the redundant subcarriers, including the DC subcarrier and repeated subcarriers, are removed by passing $\check{X}(F)$ through the redundancy removal process. However, because of the RM process at Tx (i.e., $\check{X}(F) = [\check{X}(F)/2\check{X}(F)/2]$ (see shown in Fig.1)), removing these redundant subcarriers does not cause any loss of information after compensating the first subcarrier by the middle one. Finally, the resulting signal from the redundancy removal process ($\hat{P}(F)$) is converted back to the time domain by implementing an IFFT where the output IFFT vector ($\hat{p}(t)$) passing through the PAM de-mapping and hard decision processes, to reconstruct the transmitted bits sequence.

III. SIMULATION RESULTS

The reduction of the PAPR value of OFDM in IM/DD systems was mathematically established in the previous section by implementing the FFT and RM processes before the

implementation of the IFFT method. In this section, the simulation results are presented to establish the PAPR reduction using the DFTS-OPAM scheme compared to DCO-OFDM. The PAM symbols of DFTS-OPAM are generated by separating the real and the imaginary parts of quadrature amplitude modulation (QAM) symbols [i.e., QAM symbol ($a + ib$) is separated into 'a' and 'b' PAM symbols], where these symbols are combined at the Rx to reconstruct the QAM. In this simulation study, 256 IFFT points, 16-QAM constellation, 1W white LED with PCB (HPB849KxWDx) that has 1 V linear range, Thorlabs (PDA36A-EC) PD [36], AWGN channel and 2 μ sc CP duration are considered. The PAPR values of the discrete signal is given by:

$$PAPR = \frac{\max |x_n|^2; n = 0, \dots, N - 1}{E \{ |x_n|^2 \}} \quad (11)$$

where x_n , $\max |x_n|^2$ and $E \{ |x_n|^2 \}$ are the discrete-time signal, the peak power of x_n , and the average power of x_n , respectively.

To compare the PAPRs, the complementary cumulative distribution function (CCDF) of both schemes is simulated and given in Fig. 3 whereas all the PAPR comparisons are carried out at CCDF = 10^{-4} (i.e., $\Pr\{PAPR > PAPR_0\} = 0.0001$) as in other work (e.g., in [37], [38]). Fig. 3 plots the CCDF against the PAPRs of the DFTS-OPAM and DCO-OFDM schemes. The figure demonstrates that the PAPR of the proposed scheme is ~ 7 dB lower than the PAPR value of the DCO-OFDM scheme.

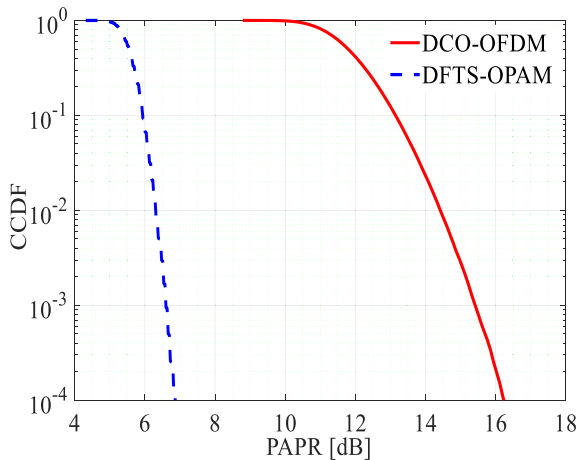


FIGURE 3. CCDF versus PAPR of the DCO-OFDM and DFTS-OPAM schemes.

Fig.4 depicts the bit error rate (BER) performance against the SNR (dB) for the DCO-OFDM and DFTS-OPAM schemes for 16-QAM. The figure shows that DCO-OFDM requires ~ 3 dB more SNR in comparison to DFTS-OPAM to achieve the BER value of 10^{-6} . This is because, only the even time-domain samples carry data in DFTS-OPAM, while all the samples are used to carry data in DCO-OFDM, making the DCO-OFDM scheme have double the spectral efficiency of DFTS-OPAM.

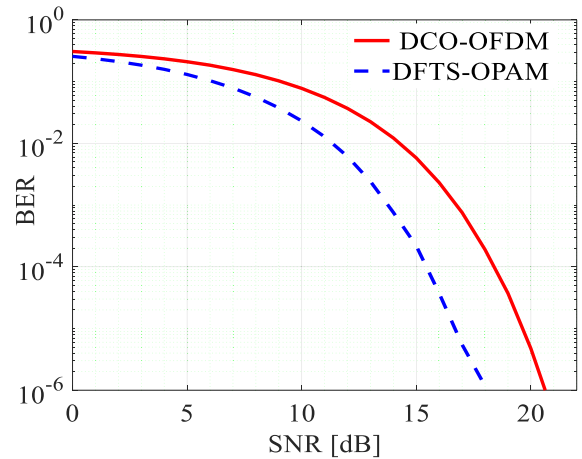


FIGURE 4. SNR versus BER for 16-QAM DCO-OFDM and 16-QAM DFTS-OPAM.

In VLC systems, the average transmitted power (P_{avg}) of the OFDM scheme is limited by the dynamic range of the LED where any signal above the LED limited linear range will be distorted or clipped, which affects the VLC system performance, since a lower P_{avg} leads to a lower SNR (i.e., leads to a shorter distance between the Tx and the Rx and/or lower constellation mapping order). Figs. 5-7 depict the maximum transmitted average power (P_{max}) that can be achieved by the two schemes. Note that P_{avg} of both schemes was varied from 0 dBm to 25 dBm in the simulations, and the error vector magnitude (EVM) was simulated at each P_{avg} value, where P_{max} is predicted to occur for EVM = 12.5%, as the system performance begins to deteriorate after this EVM% value [39], [40].

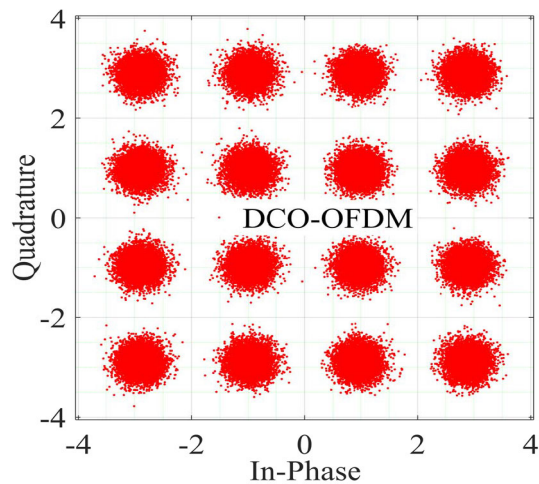


FIGURE 5. The 16-QAM constellation points of DCO-OFDM, where $P_{max} = 17.42$ dBm, EVM% = 12.5%, LED dynamic range = 1V, and only the clipping noise is considered (i.e., no AWGN).

Figs. 5 and 6 illustrate the 16-QAM constellation points of the DCO-OFDM and the DFTS-OPAM schemes, respectively for EVM = 12.5%, where only the clipping noise

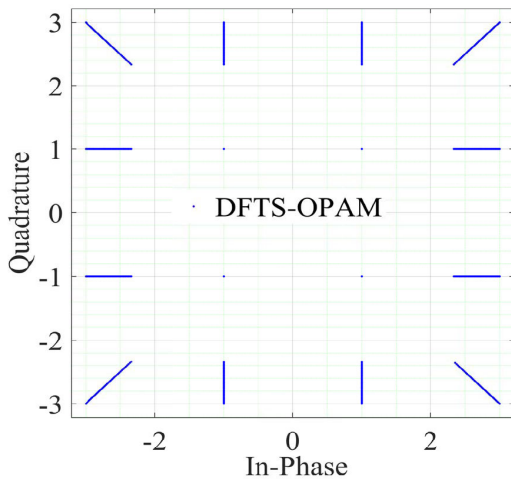


FIGURE 6. The 16-QAM constellation points of DFTS-OPAM, where $P_{max} = 19.32$, $EVM\% = 12.5\%$, LED dynamic range = 1V, and only the clipping noise is considered (i.e., no AWGN).

was considered (i.e., no AWGN) in the simulations, and the DC-bias of both schemes was set to be at the center point of the LED dynamic range (note that, the dynamic range of the LED in these simulations was 1 V). In these figures, P_{max} of the DCO-OFDM and DFTS-OPAM schemes are 17.42 dBm and 19.32 dBm, respectively (i.e., DFTS-OPAM provides approximately 2 dBm more P_{avg} in comparison to DCO-OFDM, when only the clipping noise is considered). Furthermore, Fig. 6 shows that the clipping noise in DFTS-OPAM is a linear noise.

Since the AWGN power (P_{awgn}) (i.e., the noise power of the VLC system) increases the EVM, P_{max} will be affected by the amount of P_{awgn} present in the system. Note in [30], [31], the P_{awgn} was set to -10 dBm. However, the noise power in VLC systems varies within a range as it depends on numerous parameters [1]–[3].

In Fig. 7, the P_{awgn} is varied from -15 dBm to 0 dBm, and P_{avg} of both schemes is evaluated at each P_{awgn} value to identify P_{max} , which as previously mentioned, is achieved when $EVM = 12.5\%$. From this figure, one can observe that increasing P_{awgn} decreases the P_{max} value of both schemes, as the EVM becomes more sensitive to the clipping noise by increasing the P_{awgn} level. An additional observation made from the figure is that for a 1 V LED dynamic range, the 16-QAM DCO-OFDM signaling scheme can only be implemented when the $P_{awgn} \leq -7$ dBm, as greater P_{awgn} values result in increasing the EVM beyond the 12.5% level. However, 16-QAM-DFTS-OPAM can tolerate higher noise power levels, as it can be implemented using the same given parameters for $P_{awgn} \leq -1$ dBm. Furthermore, the figure also demonstrates that the 16-QAM DFTS-OPAM scheme outperforms the 16-QAM-DCO-OFDM scheme for all noise power levels in terms of transmit power efficiency.

Finally, since LEDs are mainly used for illumination purposes, controlling the brightness of LEDs should be taken into consideration in VLC systems. One straightforward method

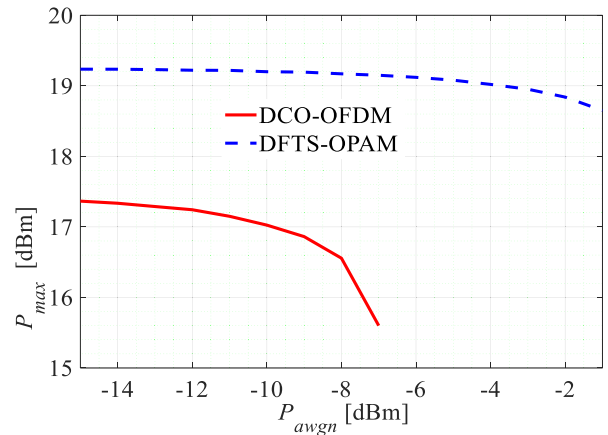


FIGURE 7. P_{max} with respect to P_{awgn} for the DCO-OFDM and DFTS-OPAM schemes, when the DC-bias is set in the middle of the LED dynamic range.

used to control the brightness of LEDs is to adjust the DC-bias level [19], [41], [42]. However, increasing or decreasing the DC-bias level results in increasing the upper or lower clipping noise of the bipolar OFDM schemes respectively. Note that, in Fig. 7, the DC-bias was set to be at the middle point of the LED linear range, thus providing a fixed illumination level.

However, to study the effect of the brightness control on the system performance of 16-QAM DFTS-OPAM and 16-QAM DCO-OFDM, the DC-bias level was set at the first and third quarter points of the LED dynamic range, thus providing three dimming control levels. The effect of setting the DC-bias at the first and third quarter points of the LED dynamic range on the system performance of the two schemes is illustrated in Figs 8 and 9, respectively. However, as both schemes are bipolar OFDM schemes, in Fig. 8, the system performance of both schemes is mostly affected by the lower clipping noise, while in Fig. 9, the upper clipping noise is the dominant clipping noise for both schemes. Furthermore, setting the DC-bias at the first quarter point of the LED linear range provides the same performance as setting it at the third quarter-point. This is because both schemes have a normal Gaussian distribution shape (i.e., the lower clipping noise in Fig.8 is the same as the upper clipping noise in Fig. 9). In addition, from these figures, it can observe that setting the DC-bias at these two points of the LED linear range makes the DCO-OFDM and DFTS-OPAM schemes only valid (i.e., $EVM > 12.5\%$) for $P_{awgn} \leq -12$ dBm and ≤ -7 dBm, respectively. Furthermore, increasing of the P_{awgn} level results in decreasing P_{max} from 13.4 dBm to 12.8 dBm, and from 12 dBm to 10.3 dBm, for 16-QAM DFTS-OPAM and 16-QAM DCO-OFDM, respectively. Note that dimming control can also be achieved in VLC systems by controlling the pulse samples duration [42]. However, since the odd samples in DFTS-OPAM do not carry any data, the duration of the even samples of this scheme have more flexibility to be adjusted according to the required illumination level, as will be demonstrated in our future work.

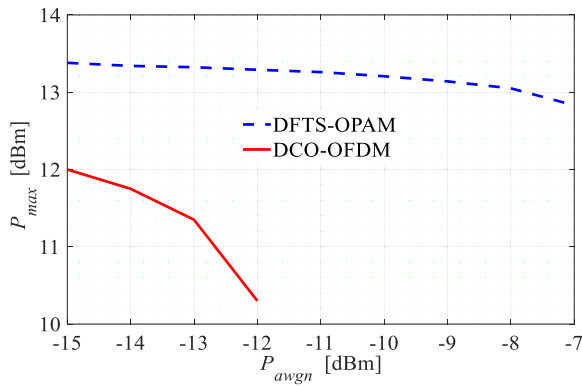


FIGURE 8. P_{max} with respect to P_{avg} for the DCO-OFDM and DFTS-OPAM schemes, when DC-bias is set at the first quarter of the LED dynamic range.

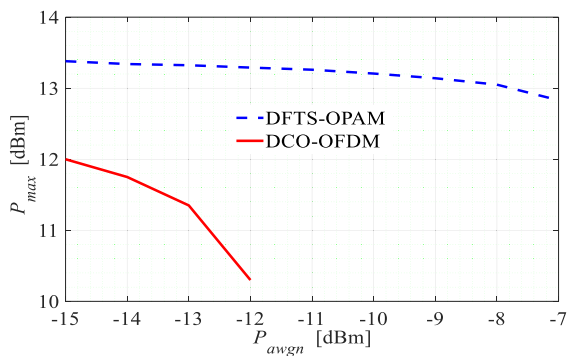


FIGURE 9. P_{max} with respect to P_{avg} for the DCO-OFDM and DFTS-OPAM schemes, when DC-bias is set at the third quarter of the LED dynamic range.

IV. EXPERIMENTAL RESULTS

The main aim of this experimental study was to implement the DFTS-OPAM signaling scheme in real time using the USRP N210 transceiver, and practically support the illustrated theory of the proposed DFTS-OPAM by practically proving low PAPR compared to DCO-OFDM in terms of providing more P_{max} , and thus increasing the distance between the Tx and Rx (de). The P_{avg} of the aforementioned two schemes are varied from 0 dBm to 24 dBm at the Tx side where the effect of this variations on the system performance was verified at the Rx.

Figs. 10 illustrate the experimental setup configuration.

The USRP transceiver was interfaced and controlled by a laptop through LabVIEW software where the main Tx and Rx parameters used are presented in Figs. 11 and 12. At the Tx, 640 and 1280 bits were randomly generated, separately mapped to 16-QAM, saved and used to implement one DFTS-OPAM block and one DCO-OFDM block respectively (i.e., 160 and 320 complex QAM data symbols for each DFTS-OPAM block and each DCO-OFDM block, respectively) where each block consists of 5 different -time domain OFDM symbols (i.e., 32 and 64-QAM data symbols used for each DFTS-OPAM time domain -symbol and DCO-OFDM time domain symbol, respectively). Note that,

for DFTS-OPAM scheme, the imaginary and the real parts of the QAM data symbols were separated to provide 64 PAM symbols before applying the FFT process.

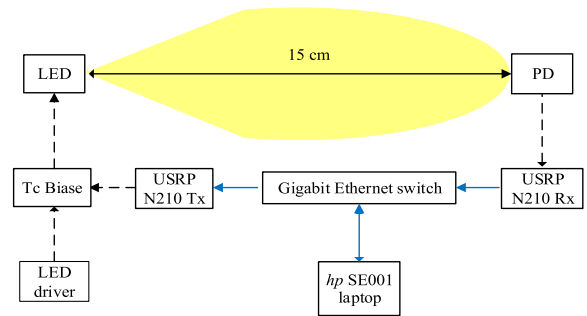


FIGURE 10. Experimental setup diagram.

As in LTE [43], to practically remove the inter-channel interference (ICI) issue, the DFTS-OPAM and the DCO-OFDM schemes were zero-padded (i.e., adding zeros at the edge of the subcarriers, before being passed to the IFFT process). As illustrated in Fig. 13, because of this process (i.e., zero-padding process) the DFTS-OPAM subcarriers are not conjugated subcarriers anymore. This result in the output IFFT samples of DFTS-OPAM complex samples. To make all DFTS-OPAM subcarriers are conjugated after the zero padding a few modifications is been done as illustrated in Fig 14.

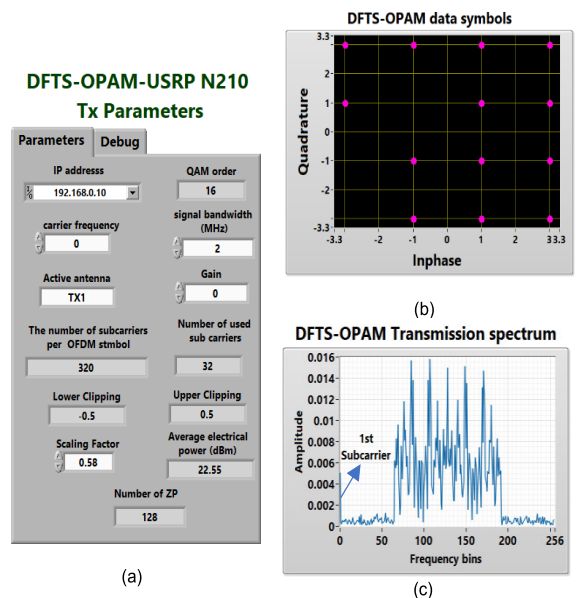


FIGURE 11. LabVIEW control panel of the USRP Tx of DFTS-OPAM, where plots (a), (b) and (c) depict the DFTS-OPAM Tx parameters, the DFTS-OPAM transmitted QAM symbols, and the DFTS-OPAM transmitted spectrum, respectively.

A 1 W white LED (HPB8-49KxWDx) introduced in the simulation section was used in this experiment where its measured L-I-V curve is shown in Fig. 15. To ensure operation in the linear region, the LED was biased at the middle point of

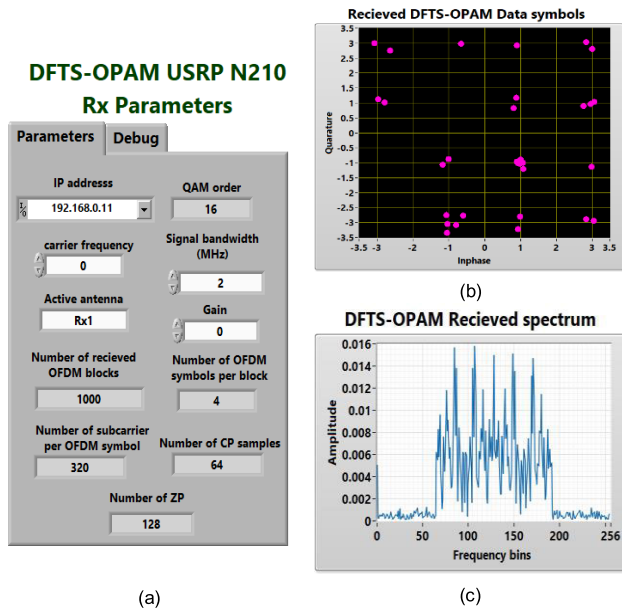


FIGURE 12. LabVIEW control panel of the USRP Rx of DFTS-OPAM, where plots (a), (b) and (c) depict the DFTS-OPAM Rx parameters, the DFTS-OPAM received QAM symbols, and the DFTS-OPAM received spectrum, respectively. Note that the 16-QAM constellation points in (b) were captured at EVM = 10.2%.

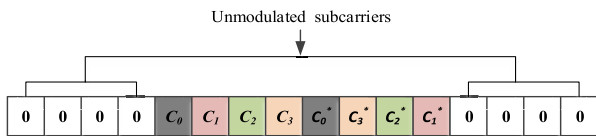


FIGURE 13. DFTS-OPAM subcarriers after inserting 8 zeros at both edges (note that in this figure, the number of subcarriers before ZP is 8).

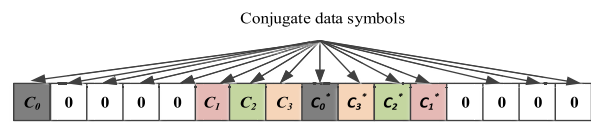


FIGURE 14. The DFTS-OPAM subcarriers after shifting the first subcarrier to the beginning.

its dynamic range (i.e., at 500 mA), providing 1 V peak to peak voltage.

At the Rx, the light signal was detected and converted back to an electrical signal by the (PDA36A-EC) PD, which is first captured by USRP Rx, then transfer to the laptop for application of signal processing and analysis (see Figs.10). 1000 OFDM blocks for each scheme were received and processed online where each block had 5 different OFDM time domain symbols and the average result was considered. The maximum likelihood (ML) algorithm was applied in this experimental work to each OFDM block for synchronization and frequency offset correction purposes, by investigating the length of the CP samples [44] (64 samples were used as CP in this work), as shown in Fig. 16.

Following the implementation of the ML algorithm, each OFDM time domain symbol was fed to the FFT process,

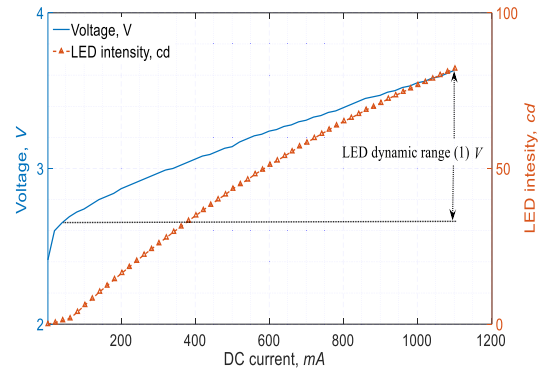


FIGURE 15. Measured L-I-V curves of the 1 W white LED (HPB8-49KxWDx).

where the redundant output subcarriers (i.e., the zero-padded and conjugate subcarriers for the DCO-OFDM scheme and the ZP and repeated subcarriers for DFTS-OPAM scheme) were rejected. Note that, because of the RM process, the first DFTS-OPAM subcarrier affected by DC-bias was replaced by the middle subcarrier in this work. Since the transmitted bits were randomly generated, saved and repeatedly transmitted, 8 subcarriers from each OFDM time domain symbol were used as the data and the pilots were investigated to estimate the transfer function of the system [3]. After estimating the transfer function of the system, the ZF algorithm was implemented to equalize the OFDM data symbols. Finally, the transmitted bits of DCO-OFDM and DFTS-OPAM were reconstructed from the equalized data symbols and saved to be processed offline by a MATLAB program for BER and EVM assessment. P_{max} of the DCO-OFDM and DFTS-OPAM schemes was experimentally evaluated by measuring the EVM at each P_{avg} value within the range $0 \leq P_{avg} \leq 24$ (note that, $P_{max} = P_{avg}$ when EVM = 12.5%). Furthermore, the benefit of the P_{max} the penalty was investigated by increasing the distance between the Tx and the Rx.

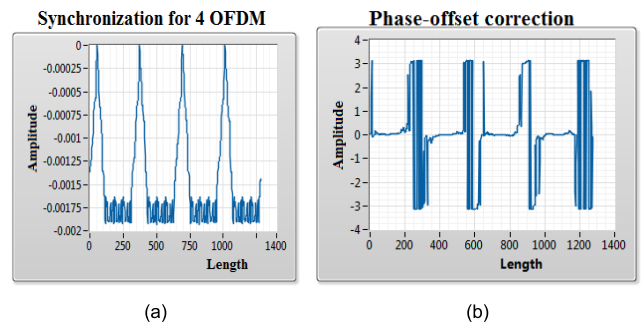


FIGURE 16. ML algorithm applied to an OFDM block to achieve: (a) synchronization estimation, and (b) frequency offset estimation.

Fig. 17 plots the EVM versus P_{avg} of the 16-QAM DCO-OFDM and 16-QAM DFTS-OPAM schemes for $d_e = 15$ cm. The figure shows that for $P_{avg} \leq 18$ dBm, the EVM of both schemes decreased by increasing P_{avg} , since the SNR is increased. However, for $P_{avg} > 18$ dBm, the EVM of

DCO-OFDM started increasing and the system performance started to deteriorate, as the linear range of the system was no longer applicable at this value. On the other hand, the system performance of DFTS-OPAM started to deteriorate by the clipping noise when $P_{avg} > 22$ dBm. The figure also demonstrates that the measured P_{max} of the DCO-OFDM and DFTS-OPAM was 20.5 dBm and 22.5 dBm, respectively (i.e., the DFTS-OPAM provided 2 dB more P_{avg} in comparison to DCO-OFDM). Furthermore, for $P_{avg} < 18$ dBm, DCO-OFDM required around 3 dB more SNR in comparison to DFTS-OPAM to achieve the same EVM % levels, since the odd samples do not carry any data in the DFTS-OPAM scheme (see Fig. 4 in the simulation results).

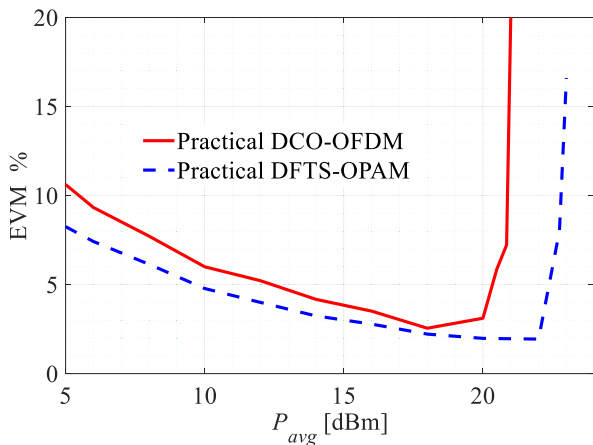


FIGURE 17. The EVM% with respect to P_{avg} for 16-QAM DCO-OFDM and 16-QAM DFTS-OPAM-FDM.

Following the previous discussions, higher P_{avg} values result in increasing the distance between the Tx and Rx. To determine the maximum achievable distance between the Tx and the Rx (d_{max}) for both schemes, P_{avg} of both schemes is set at P_{max} , de is increased progressively, and the EVM is measured at each de value, where d_{max} is achieved when $EVM = 12.5\%$ (Note that P_{max} in Fig 17 occurs for $de = 15$ cm). However, as already discussed in the simulation results (see Fig. 7), decreasing the SNR value (i.e., increasing de) reduces P_{max} . As such, for $de > 15$ cm, a lower P_{max} should be used (i.e., lower than 20.5 dBm and 22.5 dBm for DCO-OFDM and DFTS-OPAM respectively). In this investigation, P_{avg} values of 20.25 dBm and 22.25 dBm, which occurred in Fig 17 for $de = 15$ cm when $EVM = 7.5\%$, were considered as the optimum average power (P_{opt}) levels for the DCO-OFDM and DFTS-OPAM schemes respectively, as they can be used for a range of SNR values (i.e., for a range of distances).

In Fig. 18, P_{avg} of each scheme was set to its P_{opt} , de was varied within the range $15 \text{ cm} \leq de \leq 70 \text{ cm}$, and the EVM was measured after each 2 cm. From this figure, it can be seen that the EVM of DCO-OFDM and DFTS-OPAM reach the threshold value (i.e., $EVM = 12.5\%$) for $de = 43$ cm and 63 cm , respectively. As such, implementing the

proposed scheme increased de by up to 44% in comparison to the traditional DCO-OFDM scheme. Note that, in Fig 18, to ensure that the achieved distance is the maximum one for both schemes, P_{avg} of both schemes was kept around their P_{opt} values, and d_{max} was achieved when $P_{avg} = P_{opt}$.

Finally, the BER performance of the two schemes was investigated experimentally as a function of de , as illustrated in Fig. 19, where P_{avg} of both schemes was set at their P_{opt} . The figure demonstrates that for $de < 45$ cm, both schemes achieved the same BER performance (i.e., both schemes reached the noise floor), as the EVM of the two schemes was less than 12.5% for shorter distances. However, for $de \geq 45$ cm, the BER performance of DCO-OFDM is being affected as its SNR is dropped down and consequently, the EVM become more than 12.5% while the BER performance of the DFTS-OPAM scheme is start being affected when $de > 65$ cm, which is because the P_{avg} of the proposed scheme is around 2 dBm more than the P_{avg} of the traditional DCO-OFDM.

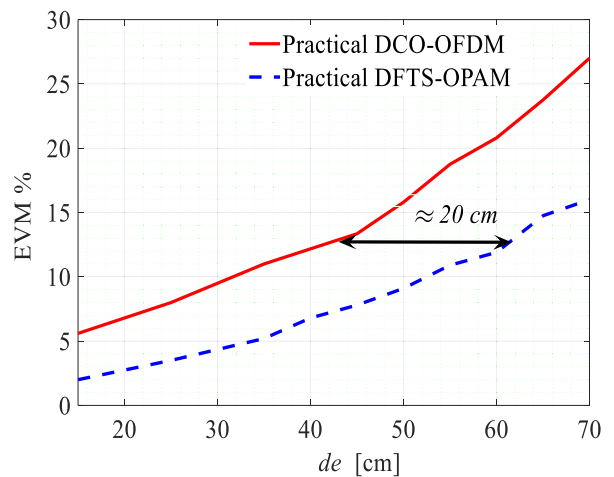


FIGURE 18. EVM% versus de for the 16-QAM DCO-OFDM and 16 QAM DFTS-OPAM schemes, where P_{avg} of DCO-OFDM and DFTS-OPAM is 20.25 dBm and 22.25 dBm, respectively.

Nevertheless, in a real scenario, the VLC link distance between the Tx and the Rx should be > 150 cm [1], [2], [19]. In fact, VLC link distance depends on several parameters such as: transmitted average power, divergence angle at the Tx, Rx field of view (FOV), Rx sensitivity, measuring devices, amplifier at the Rx, optical filter, Rx non-imaging concentrator internal reflective index, modulation depth, data rate, etc. [2], [45]. Note, because of the limited optical wireless communication Lab equipment that we have and because the main reason behind this work is to introduce the new novel DFTS-OPAM scheme first time and compare it with the known DCO-OFDM scheme in term of their PAPR for the same given parameters, we have by MATLAB simulation proven that changing few parameters (i.e., LED semi angle at half-power ($\theta/2$), QAM order and Non-imaging concentrator internal reflective index) on our practical experiment

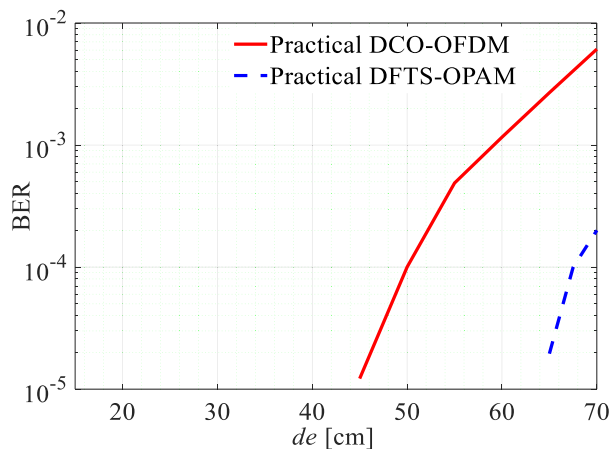


FIGURE 19. The BER with respect to d_e for both 16-QAM DCO-OFDM and 16-QAM DFTS-OPAM where, P_{avg} of DCO-OFDM and DFTS-OPAM are 20.25 dBm and 22.25 dBm, respectively.

TABLE 1. VLC simulation parameters.

Parameters	Value
Number of iterations	10^6
LED Type	1W white LED with PCB (HPB849KxWDx)
LED bandwidth	2MHz
LED linearity	~ 1 V
Photodetector (PD)	Thorlab (PDA36A-EC)
PD bandwidth	10 MHz
PD noise (RMS)	$300 \mu\text{V}$
PD responsivity	0.65 A/W
PD active area	16 mm^2
Rx FOV	20°

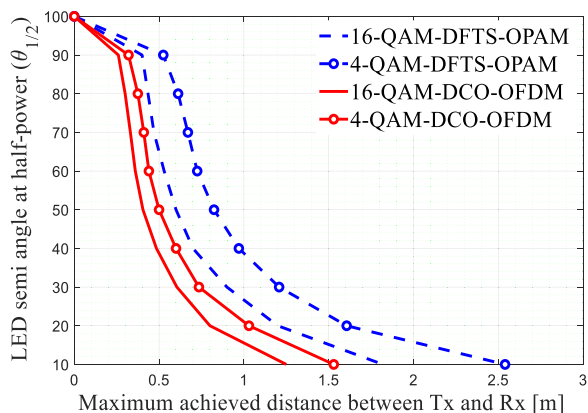


FIGURE 20. d_{max} versus $\theta_{1/2}$ for 16-QAM DFTS-OPAM, 4-QAM DFTS-OPAM, 16-QAM DCO-OFDM and 4-QAM DCO-OFDM

can increase the maximum achievable distance between the Tx and the Rx to be more than 150 cm as illustrated in Figures 20, 21 and 22 at the Appendix Section where the VLC simulation parameters that were used for these plots are also illustrated at the same Section in Table 1.

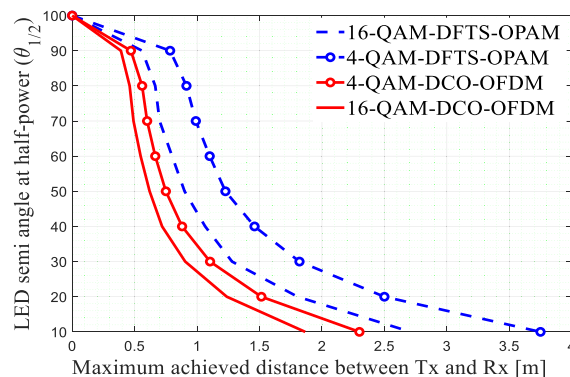


FIGURE 21. d_{max} versus $\theta_{1/2}$ for 16-QAM DFTS-OPAM, 4-QAM DFTS-OPAM, 16 QAM DCO-OFDM and 4 QAM-DCO-OFDM when 1.5 non-imaging concentrator internal reflective index is used at the Rx.

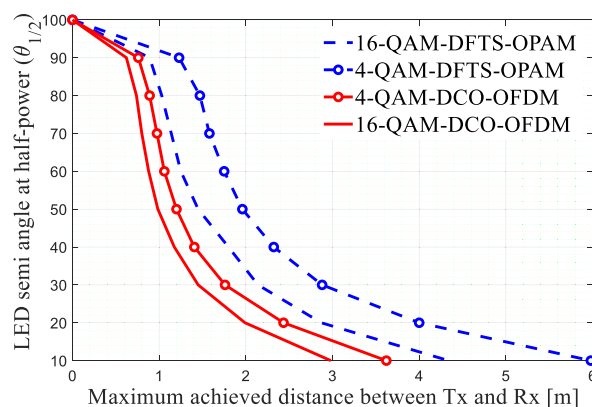


FIGURE 22. d_{max} versus $\theta_{1/2}$ for 16-QAM DFTS-OPAM, 4-QAM DFTS-OPAM, 16-QAM DCO-OFDM and 4-QAM DCO-OFDM when 2.4 non-imaging concentrator internal reflective index is used at the Rx.

V. CONCLUSION

The proposed DFTS-OPAM were introduced in this paper to significantly improve the PAPR of the OFDM signal in IM/DD based VLC systems, by making SC-IFDMA scheme suitable for IM/DD without any HS requirements. This IM/DD compatibility is achieved in DFTS-OPAM by replacing the interleaving mapping block in the SC-IFDMA Tx by the RM block and using PAM as a modulation scheme. As such, the output time domain samples of the IFFT are bipolar real samples that have as low PAPR as that of the SCM scheme. The simulation results of DFTS-OPAM showed that the PAPR value of DFTS-OPAM is 7 dB lower than the PAPR value of the traditional DCO-OFDM scheme. The results also showed that the DCO-OFDM requires 3 dB more SNR in comparison to DFTS-OPAM to achieve the same BER performance. The impact of this PAPR reduction on the system performance was experimentally investigated, where the results showed that the maximum achieved distance between the Tx and Rx was increased by up to 44% when the DFTS-OPAM scheme was implemented compared to DCO-OFDM.

APPENDIX

See Table 1 and Figs. 20–22.

REFERENCES

- [1] P. A. Hoeher, *Visible Light Communications: Theoretical and Practical Foundations*. Munich, Germany: Hanser Fachbuch, 2019.
- [2] Z. Ghassemlooy, L. N. Alves, S. Zvanovec, and M. Khalighi, *Visible Light Communications: Theory and Applications*. Boca Raton, FL, USA: CRC Press, 2017.
- [3] O. Saied, "Orthogonal frequency division multiplexing for indoor visible light communication links," Ph.D. dissertation, Dept. Eng. Environ., Northumbria Univ., Newcastle upon Tyne, U.K., 2018.
- [4] M. Uysal, F. Miramirkhani, O. Narmanlioglu, T. Baykas, and E. Panayirci, "IEEE 802.15.7r1 reference channel models for visible light communications," *IEEE Commun. Mag.*, vol. 55, no. 1, pp. 212–217, Jan. 2017, doi: 10.1109/MCOM.2017.1600872CM.
- [5] S.-W. Wang, F. Chen, L. Liang, S. He, Y. Wang, X. Chen, and W. Lu, "A high-performance blue filter for a white-led-based visible light communication system," *IEEE Wireless Commun.*, vol. 22, no. 2, pp. 61–67, Apr. 2015, doi: 10.1109/MWC.2015.7096286.
- [6] N. Fujimoto and S. Yamamoto, "The fastest visible light transmissions of 662 Mb/s by a blue LED, 600 Mb/s by a red LED, and 520 Mb/s by a green LED based on simple OOK-NRZ modulation of a commercially available RGB-type white LED using pre-emphasis and post-equalizing techniques," in *Proc. Eur. Conf. Opt. Commun. (ECOC)*, Cannes, France, Sep. 2014, pp. 1–3, doi: 10.1109/ECOC.2014.6963895.
- [7] X. Huang, Z. Wang, J. Shi, Y. Wang, and N. Chi, "1.6 Gbit/s phosphorescent white LED based VLC transmission using a cascaded pre-equalization circuit and a differential outputs PIN receiver," *Opt. Exp.*, vol. 23, no. 17, pp. 22-34–22-42, Aug. 2015, doi: 10.1364/OE.23.022034.
- [8] H. Li, X. Chen, J. Guo, and H. Chen, "A 550 Mbit/s real-time visible light communication system based on phosphorescent white light LED for practical high-speed low-complexity application," *Opt. Exp.*, vol. 22, no. 22, pp. 27203–27213, 2014, doi: 10.1364/OE.22.027203.
- [9] P. A. Haigh, Z. Ghassemlooy, S. Rajbhandari, I. Papakonstantinou, and W. Popoola, "Visible light communications: 170 Mb/s using an artificial neural network equalizer in a low bandwidth white light configuration," *J. Lightw. Technol.*, vol. 32, no. 9, pp. 1807–1813, May 15, 2014, doi: 10.1109/JLT.2014.2314635.
- [10] X. Li, Z. Ghassemlooy, S. Zvanovec, R. Perez-Jimenez, and P. A. Haigh, "Should analogue pre-equalisers be avoided in VLC systems?" *IEEE Photon. J.*, vol. 12, no. 2, pp. 1–14, Apr. 2020, doi: 10.1109/JPHOT.2020.2966875.
- [11] T. Fath and H. Haas, "Performance comparison of MIMO techniques for optical wireless communications in indoor environments," *IEEE Trans. Commun.*, vol. 61, no. 2, pp. 733–742, Feb. 2013, doi: 10.1109/TCOMM.2012.120512.110578.
- [12] Y. Hong, T. Wu, and L.-K. Chen, "On the performance of adaptive MIMO-OFDM indoor visible light communications," *IEEE Photon. Technol. Lett.*, vol. 28, no. 8, pp. 907–910, Apr. 15, 2016, doi: 10.1109/LPT.2016.2517192.
- [13] O. Narmanlioglu, R. C. Kizilirmak, T. Baykas, and M. Uysal, "Link adaptation for MIMO OFDM visible light communication systems," *IEEE Access*, vol. 5, pp. 26006–26014, 2017, doi: 10.1109/ACCESS.2017.2771333.
- [14] M. Wolf and M. Haardt, "On the DC balance of multi-level PAM VLC systems," in *Proc. 21st Int. Conf. Transparent Opt. Netw. (ICTON)*, Angers, France, Jul. 2019, pp. 1–5, doi: 10.1109/ICTON.2019.8840531.
- [15] A. Nuwanpriya, S.-W. Ho, J. A. Zhang, A. J. Grant, and L. Luo, "PAM-SCFDE for optical wireless communications," *J. Lightw. Technol.*, vol. 33, no. 14, pp. 2938–2949, Jul. 15, 2015, doi: 10.1109/JLT.2015.2424456.
- [16] R. Bian, I. Tavakkolnia, and H. Haas, "15.73 Gb/s visible light communication with off-the-shelf LEDs," *J. Lightw. Technol.*, vol. 37, no. 10, pp. 2418–2424, May 15, 2019, doi: 10.1109/JLT.2019.2906464.
- [17] O. Saied, Z. Ghassemlooy, X. Tang, X. Dai, H. L. Minh, and B. Lin, "Position encoded asymmetrically clipped optical orthogonal frequency division multiplexing in visible light communications," *J. Commun. Inf. Netw.*, vol. 2, no. 4, pp. 1–10, Dec. 2017, doi: 10.1007/s41650-017-0038-2.
- [18] V. Kishore, V. S. Prasad, and V. V. Mani, "A blind timing synchronization algorithm for DCO-OFDM VLC systems," *IEEE Photon. Technol. Lett.*, vol. 32, no. 17, pp. 1121–1124, Sep. 1, 2020, doi: 10.1109/LPT.2020.3013447.
- [19] S. Dimitrov and H. Haas, *Principles of LED Light Communications: Towards Networked Li-Fi*. Cambridge, U.K.: Cambridge Univ. Press, 2015.
- [20] J. Armstrong and A. J. Lowery, "Power efficient optical OFDM," *Electron. Lett.*, vol. 42, no. 6, pp. 370–372, Mar. 2006, doi: 10.1049/el:20063636.
- [21] S. C. J. Lee, S. Randel, F. Breyer, and A. M. J. Koonen, "PAM-DMT for intensity-modulated and direct-detection optical communication systems," *IEEE Photon. Technol. Lett.*, vol. 21, no. 23, pp. 1749–1751, Dec. 1, 2009, doi: 10.1109/LPT.2009.2032663.
- [22] D. Tsonev, S. Sinanovic, and H. Haas, "Pulse shaping in unipolar OFDM-based modulation schemes," in *Proc. IEEE Globecom Workshops*, Anaheim, CA, USA, Dec. 2012, pp. 1208–1212, doi: 10.1109/GLOCOMW.2012.6477752.
- [23] H. Myung, J. Lim, and D. Goodman, "Peak-to-average power ratio of single carrier FDMA signals with pulse shaping," in *Proc. IEEE 17th Int. Symp. Pers., Indoor Mobile Radio Commun.*, Helsinki, Finland, Sep. 2006, pp. 1–5, doi: 10.1109/PIMRC.2006.254407.
- [24] J. Zyren. (Sep. 2007). *White Paper: Overview of the 3GPP Long Term Evolution Physical Layer*. Austin, TX, USA. White Paper. Freescale Semiconductor. [Online]. Available: <https://www.nxp.com/docs/en/whitepaper/3GPPEVOLUTIONNWP.pdf>
- [25] J. Kim and H.-G. Ryu, "Adaptive modulation for maximum throughput of multi-user SC-FDMA system in doubly selective channel," in *Proc. IEEE Radio Wireless Symp. (RWS)*, Jan. 2010, pp. 681–684, doi: 10.1109/RWS.2010.5434143.
- [26] J. Yuan, Y. Du, L. Going, and J. Li, "A bit-loading algorithm in SC-FDE system," in *Proc. IEEE Radio Wireless Symp.*, Oct. 2006, pp. 27–30, doi: 10.1109/RWS.2006.1615086.
- [27] A. Ahmad, "Resource allocation and adaptive modulation in uplink SC-FDMA systems," *Wireless Pers. Commun.*, vol. 75, no. 4, pp. 2217–2242, Apr. 2014.
- [28] M. Al-Rawi, R. Jantti, J. Torsner, and M. Sagfors, "Opportunistic uplink scheduling for 3G LTE systems," in *Proc. Innov. Inf. Technol. (IIT)*, Nov. 2007, pp. 705–709, doi: 10.1109/IIT.2007.4430425.
- [29] K. Acolatse, Y. Bar-Ness, and S. K. Wilson, "Novel techniques of single-carrier frequency-domain equalization for optical wireless communications," *EURASIP J. Adv. Signal Process.*, vol. 2011, no. 1, pp. 1–13, Dec. 2011, doi: 10.1155/2011/393768.
- [30] R. Mesleh, H. Elgala, and H. Haas, "LED nonlinearity mitigation techniques in optical wireless OFDM communication systems," *IEEE/OSA J. Opt. Commun. Netw.*, vol. 4, no. 11, pp. 865–875, Nov. 2012, doi: 10.1364/JOCN.4.000865.
- [31] O. Saied, Z. Ghassemlooy, S. Zvanovec, R. C. Kizilirmak, and B. Lin, "Unipolar-pulse amplitude modulation frequency division multiplexing for visible light communication systems," *Opt. Eng.*, vol. 59, no. 9, Sep. 2020, Art. no. 096108, doi: 10.1117/1.OE.59.9.096108.
- [32] C. Wu, H. Zhang, and W. Xu, "On visible light communication using LED array with DFT-spread OFDM," in *Proc. IEEE Int. Conf. Commun. (ICC)*, Sydney, NSW, Australia, Jun. 2014, pp. 3325–3330, doi: 10.1109/ICC.2014.6883834.
- [33] O. Saied, Z. Ghassemlooy, R. C. Kizilirmak, X. Dai, C. Ribeiro, M. Zhang, and S. Rajbhandari, "Single carrier optical FDM in visible light communication," in *Proc. 10th Int. Symp. Commun. Syst., Netw. Digit. Signal Process. (CSNDSP)*, Prague, Czech Republic, Jul. 2016, pp. 1–5, doi: 10.1109/CSNDSP.2016.7573947.
- [34] A. W. Azim, Y. Le Guennec, and G. Maury, "Hermitian symmetry free optical-single-carrier frequency division multiple access for visible light communication," *Opt. Commun.*, vol. 415, pp. 177–185, May 2018, doi: 10.1016/j.optcom.2018.01.036.
- [35] O. Saied, Z. Ghassemlooy, S. Rajbhandari, and A. Burton, "Optical single carrier-interleaved frequency division multiplexing for visible light communication systems," *Optik*, vol. 194, pp. 1–7, 2019, doi.org/10.1016/j.ijleo.2019.06.010.
- [36] THORLABS. *PDA36A-EC—Si Switchable Gain Detector, 350-1100 nm, 10 MHz BW, 13 mm2, M4 Taps*, 2006. [Online]. Available: <https://www.thorlabs.com/catalogpages/obsolete/2018/PDA36AEC.pdf>.

- [37] T. Zhang, H. Ji, Z. Ghassemlooy, X. Tang, B. Lin, and S. Qiao, "Spectrum-efficient triple-layer hybrid optical OFDM for IM/DD-based optical wireless communications," *IEEE Access*, vol. 8, pp. 10352–10362, 2020, doi: [10.1109/ACCESS.2020.2964792](https://doi.org/10.1109/ACCESS.2020.2964792).
- [38] J. G. Doblado, A. C. O. Oria, V. Baena-Lecuyer, P. Lopez, and D. Perez-Calderon, "Cubic metric reduction for DCO-OFDM visible light communication systems," *J. Lightw. Technol.*, vol. 33, no. 10, pp. 1971–1978, May 15, 2015, doi: [10.1109/JLT.2015.2402755](https://doi.org/10.1109/JLT.2015.2402755).
- [39] X. Liu, F. Effenberger, N. Chand, L. Zhou, and H. Lin, "Demonstration of bandwidth-efficient mobile fronthaul enabling seamless aggregation of 36 E-UTRA-like wireless signals in a single 1.1-GHz wavelength channel," in *Proc. Opt. Fiber Commun. Conf.*, Los Angeles, CA, USA, 2015, pp. 1–3.
- [40] H. Li, R. Hu, Q. Yang, M. Luo, Z. He, P. Jiang, Y. Liu, X. Li, and S. Yu, "Improving performance of mobile fronthaul architecture employing high order delta-sigma modulator with PAM-4 format," *Opt. Exp.*, vol. 25, no. 1, pp. 1–9, 2017, doi: [10.1364/OE.25.000001](https://doi.org/10.1364/OE.25.000001).
- [41] S. Yao and X. Zhang, "Joint beamforming and DC bias optimization in VLC with dimming control," in *Proc. IEEE 85th Veh. Technol. Conf. (VTC Spring)*, Jun. 2017, pp. 1–5, doi: [10.1109/VTCSpring.2017.8108581](https://doi.org/10.1109/VTCSpring.2017.8108581).
- [42] R. C. Kizilirmak and Y. H. Kho, "On the brightness control of ACO-OFDM based VLC systems," in *Proc. 9th Int. Conf. Sens. Technol. (ICST)*, Dec. 2015, pp. 215–218, doi: [10.1109/ICSensT.2015.7438395](https://doi.org/10.1109/ICSensT.2015.7438395).
- [43] S. C. Yang, *OFDMA System Analysis and Design*. Norwood, MA, USA: Artech House, 2010.
- [44] J.-J. van de Beek, M. Sandell, and P. O. Borjesson, "ML estimation of time and frequency offset in OFDM systems," *IEEE Trans. Signal Process.*, vol. 45, no. 7, pp. 1800–1805, Jul. 1997, doi: [10.1109/78.599949](https://doi.org/10.1109/78.599949).
- [45] J. M. Kahn and J. R. Barry, "Wireless infrared communications," *Proc. IEEE*, vol. 85, no. 2, pp. 265–298, Feb. 1997, doi: [10.1109/5.554222](https://doi.org/10.1109/5.554222).



XINGWANG LI (Senior Member, IEEE) received the M.Sc. degree from the University of Electronic Science and Technology of China, in 2010, and the Ph.D. degree from the Beijing University of Posts and Telecommunications, in 2015. From 2010 to 2012, he worked at Comba Telecom Ltd., Guangzhou, China, as an Engineer. He spent one year, from 2017 to 2018, as a Visiting Scholar at Queen's University Belfast, Belfast, U.K. He is also a Visiting Scholar at the State Key Laboratory of Networking and Switching Technology, Beijing University of Posts and Telecommunications, from 2016 to 2018. He is currently an Associate Professor with the School of Physics and Electronic Information Engineering, Henan Polytechnic University, Jiaozuo, China. His research interests include MIMO communication, cooperative communication, hardware constrained communication, non-orthogonal multiple access, physical layer security, unmanned aerial vehicles, and the Internet of Things. He has served as a TPC Member for many conferences, such as the IEEE GLOBECOM, IEEE WCNC, IEEE VTC, and IEEE ICC. He has also served as the Co-Chair for the IEEE/IET CSNDSP 2020 of the Green Communications and Networks Track. He also serves as an Editor on the Editorial Board for *IEEE Access*, *Computer Communications*, *Physical Communication*, *KSII Transactions on Internet and Information Systems*, *IET Networks*, and *IET Quantum Communication*. He is also the Lead Guest Editor for the Special Issue on UAV-Enabled B5G/6G Networks: Emerging Trends and Challenges of *Physical Communication*, the Special Issue on Recent Advances in Physical Layer Technologies for the 5G-Enabled Internet of Things of *Wireless Communications and Mobile Computing*, and the Special Issue on Recent Advances in Multiple Access for 5G-Enabled IoT of *Security and Communication Networks*.



KHALED M. RABIE (Senior Member, IEEE) received the M.Sc. and Ph.D. degrees in electrical and electronic engineering from The University of Manchester, in 2011 and 2015, respectively. He is currently a Senior Lecturer with the Department of Engineering, Manchester Metropolitan University (MMU), U.K. He has worked as a part of several large scale industrial projects and has published over 150 journals and conference papers (mostly IEEE). His current research interest includes the next-generation wireless communication systems. He is also a fellow of the U.K. Higher Education Academy (FHEA). He serves regularly on the technical program committee (TPC) for several major IEEE conferences, such as GLOBECOM, ICC, and VTC. He has received many awards over the past few years in recognition of his research contributions including the Best Paper Award at the 2021 IEEE CITS, the IEEE Access Editor of the Month Award for August 2019, and the Best Student Paper Award at the 2015 IEEE ISPLC. He is currently serving as an Editor for *IEEE COMMUNICATIONS LETTERS*, an Editor for *IEEE Internet of Things Magazine*, an Associate Editor for *IEEE Access*, an Area Editor for *Physical Communication* (Elsevier), and an Executive Editor for the *Transactions on Emerging Telecommunications Technologies* (Wiley). He also guest-edited many special issues in journals, including *IEEE Wireless Communications Magazine*, *IEEE Access*, *Electronics*, and *Sensors*.



OSAMA SAIED received the Higher Diploma degree (Hons.) in electronic engineering from the High Institute for Poly Technics, Garyan, Libya, in 2000, the M.Sc. degree in communication and signal processing from Newcastle University, Newcastle upon Tyne, U.K., in 2010, and the Ph.D. degree in visible light communications from Northumbria University, Newcastle upon Tyne, in 2018. He has been working as a Networking Engineer with the Biruni Remote Sensing Center, Tripoli, Libya, since 2001. He has published five journal articles and one conference paper. His research interests include optical wireless communications, free-space optics, visible light communications, and RF over optics.